Biomimetic channel modeling local vascular dynamics of pro-inflammatory endothelial changes

Antony Thomas,[1,a)] H. Daniel Ou-Yang,[1,2,a)] Linda Lowe-Krentz,[1,3,a)] Vladimir R. Muzykantov,[4,a)] and Yaling Liu[1,5,b)]
[1]*Bioengineering Program, Lehigh University, Bethlehem, Pennsylvania 18015, USA*
[2]*Department of Physics, Lehigh University, Bethlehem, Pennsylvania 18015, USA*
[3]*Department of Biological Sciences, Lehigh University, Bethlehem, Pennsylvania 18015, USA*
[4]*Institute for Translational Medicine and Therapeutics, University of Pennsylvania School of Medicine, Philadelphia, Pennsylvania 19104, USA*
[5]*Department of Mechanical Engineering and Mechanics, Lehigh University, Bethlehem, Pennsylvania 18015, USA*

(Received 16 August 2015; accepted 16 November 2015; published online 6 January 2016)

Endothelial cells form the inner lining of blood vessels and are exposed to various factors like hemodynamic conditions (shear stress, laminar, and turbulent flow), biochemical signals (cytokines), and communication with other cell types (smooth muscle cells, monocytes, platelets, etc.). Blood vessel functions are regulated by interactions among these factors. The occurrence of a pathological condition would lead to localized upregulation of cell adhesion molecules on the endothelial lining of the blood vessel. This process is promoted by circulating cytokines such as tumor necrosis factor-alpha, which leads to expression of intercellular adhesion molecule-1 (ICAM-1) on the endothelial cell surface among other molecules. ICAM-1 is critical in regulating endothelial cell layer dynamic integrity and cytoskeletal remodeling and also mediates direct cell-cell interactions as part of inflammatory responses and wound healing. In this study, we developed a biomimetic blood vessel model by culturing confluent, flow aligned, endothelial cells in a microfluidic platform, and performed real time *in situ* characterization of flow mediated localized pro-inflammatory endothelial activation. The model mimics the physiological phenomenon of cytokine activation of endothelium from the tissue side and studies the heterogeneity in localized surface ICAM-1 expression and F-actin arrangement. Fluorescent antibody coated particles were used as imaging probes for identifying endothelial cell surface ICAM-1 expression. The binding properties of particles were evaluated under flow for two different particle sizes and antibody coating densities. This allowed the investigation of spatial resolution and accessibility of ICAM-1 molecules expressed on the endothelial cells, along with their sensitivity in receptor-ligand recognition and binding. This work has developed an *in vitro* blood vessel model that can integrate various heterogeneous factors to effectively mimic a complex endothelial microenvironment and can be potentially applied for relevant blood vessel mechanobiology studies. [http://dx.doi.org/10.1063/1.4936672]

INTRODUCTION

The endothelial cell monolayer lining the inner layer of blood vessels is an interface between blood and tissues. Under disease conditions, pathological mediators cause endothelial activation manifested by expression of cell adhesion molecules, among other signs.[1] The local

[a)]Electronic addresses: ant210@lehigh.edu; hdo0@lehigh.edu; ljl0@lehigh.edu; and muzykant@mail.med.upenn.edu.
[b)]Author to whom correspondence should be addressed. Electronic mail: yal310@lehigh.edu. Tel.: +1-610-758-5839. Fax: +1-610-758-6224.

vascular dynamics of these changes and their induction remain largely enigmatic, in part due to the difficulties of modeling. *In vivo* studies most adequately reflect the pathophysiological context, but the system complexity is beyond our current means to accurately dissect specific aspects. Parameters of the heterogeneous physical, chemical, and biological pathways influencing the blood vessel add to the complexity.[2] On the other hand, the biological relevance of conventional cell culture models is limited. Therefore, both understanding of pathophysiology and designing adequate interventions demand alternative bio-mimetic model platforms.

An *in vitro* bio-mimetic blood vessel should be able to model *in vivo* physiological characteristics, relevant flow dynamics, vessel shape/dimensions, and localized pathology microenvironment. Microfluidic engineering enables integration of precisely controlled flow in channels, whose shape and dimensions can be designed to requirement with resolution limits in the micron scale. There are a few *in vitro* reports using microfluidic chips to study vascular functions.[3–12] Work by Tsou *et al.* employed soft lithography based flow chamber to study how endothelial cells sense a gradient of flow shear stress (FSS) and tumor necrosis factor-alpha (TNF-α) triggering to transduce signals that regulate membrane expression of cell adhesion molecules and monocyte recruitment.[13] Sato *et al.* used a microfluidic model separated by a membrane containing both blood and lymphatic vessels for examining vascular permeability.[9] Kim *et al.*[4] studied cytokine mediated controlled permeability on endothelial cell layers through nanoparticle (NP) extravasation. However, this study was performed under static conditions without consideration of the FSS conditions to which the endothelium would have been exposed *in vivo*. This model also lacked the ability to apply localized cytokine challenge to the endothelial cell layer. Other vascular blood vessel systems did incorporate FSS,[14,15] yet were limited to testing a single condition at a time.

This study aims to develop a bio-mimetic blood vessel to study dynamics of intercellular adhesion molecule-1 (ICAM-1) expression on the luminal surface of endothelial cells induced by local action of pro-inflammatory cytokines. To achieve this goal, we combined endothelial microfluidics/flow adaptation approach with local cytokine application via a semi-permeable "sub-endothelial compartment" and employed antibody-coated NPs as imaging probes. This approach allowed us to define flow-mediated local heterogeneity of endothelial activation by cytokines that appears to reflect the pathophysiology of the process. The platform facilitated real-time microscopic analysis of cellular characteristics and particle binding, as well as differentiated between localized differences in cell responses to treatment. This is a reliable and relatively simple methodology to quantitatively assess this functional parameter without using radioisotope labeled ICAM-1 antibodies, which is associated with regulatory, safety, and financial difficulties. Comparing with western-blotting and polymerase chain reaction analyzes, using targeted NPs is advantageous because it detects selectively fraction of ICAM-1 molecules that is exposed on the cell surface. They are also less prone to non-specific adhesion to cell surface under flow compared to bare antibody due to its relatively larger size. In addition, this formulation can be used for targeted drug delivery to endothelium, the research direction that our team pursues beyond the framework of the present investigation.

MATERIALS AND METHODS

Fabrication of bio-mimetic blood vessel model

Blood vessel-mimicking channels were photolithographically fabricated on a silicon wafer and cast out of polydimethylsiloxane (PDMS). The master for fabricating the channels was patterned on a silicon wafer using SU-8 2050 photoresist (MicroChem Corp.). Sylgard 184 PDMS (Dow Corning Corp.) was prepared according to manufacturer's instruction and cast over the photoresist pattern. The blood vessel model developed in this study has an upper and lower channel separated by a semi-permeable, cell culture friendly membrane. This dual channel design allows localized TNF-α treatment from the lower channel on the endothelial cell layer growing in the upper channel. The upper channel was 350 μm wide and 100 μm high, and the lower channel was 1000 μm wide and 100 μm high. A polycarbonate, track-etched thin clear membrane (Whatman, GE Healthcare) with 1 μm diameter pores and an average calculated pore

density of 1.5×10^7 pores/cm^2 was embedded between two PDMS channels. The protocol for fabricating the device has been detailed in previous publications.[16–18] The PDMS slabs containing the upper and lower channels were carefully peeled off the master template. The property of PDMS was tuned to be more cell culture friendly by extended baking (4 h at 80 °C) to ensure complete cross linking of monomers,[19] and any leftover monomers were extracted by soaking them in ethanol overnight.[20] The lower PDMS channel was kept thin to facilitate microscopy based imaging using a high magnification objective. This layer is bonded on a thin glass slide by exposing the sides in contact to oxygen plasma. Upper and lower PDMS channels were bonded to the membrane using a thin PDMS mortar film. The mortar film was a mixture of PDMS prepolymer (10:1 ratio of base and curing agent) with toluene in equal proportion, and a thin layer (∼2–3 μm) was obtained by spin-coating this on a glass slide at 1500 rpm for 60 s. PDMS channel sides were stamped onto this thin film. The device was then assembled with the membrane in between the PDMS slabs and making sure the channels were aligned. After assembly, the device was placed in an oven at 60 °C overnight for curing the PDMS mortar, and the integrity of the device was ensured before seeding cells. Inlet and outlet ports were punched to provide access to upper and lower channels.

Preparation and characterization of anti-ICAM-1 coated particles

Neutravidin coated 210 nm and 1 μm fluorescent particles (Invitrogen Corp.) were diluted to 10^{10} and 10^9 particles/ml, respectively, using BlockAid^{TM} solution (Invitrogen Corp.) and sonicated. Biotinylated Protein G (29988, Thermo Scientific) diluted in 1% bovine serum albumin (BSA) solution was bound to the NeutrAvidin coating on the particles initially. The particles were incubated for 12 h in a shaker at 4 °C, and the unbound protein G was removed by centrifugation. For ICAM-1 coating, bovine-specific anti-ICAM-1 antibodies (0.2 mg/ml in 1%BSA/phosphate buffered saline) raised in mice (NB500-318, Novus Biologicals) were incubated with the Protein G coated particles for 12 h in a shaker at 4 °C, and the unbound antibody was removed by centrifugation. The particles were also washed in 1% BSA solution to remove any leftover unbound antibody, and finally the particles were diluted to their respective working concentrations (Table I). The concentration of the particles available was analyzed on a microplate reader at 485 nm excitation/530 nm emission and compared to a calibration curve constructed from stock particle solution.

The anti-ICAM-1 coating density on the particle was determined using an ELISA. 210 nm particles were conjugated with anti-ICAM-1 at 100% (possible maximum) and 50% of coating density (obtained by decreasing the anti-ICAM-1 antibody to 0.1 mg/ml and adding goat control IgG (AB-108-C, R&D Systems) at 0.1 mg/ml during the coating process), while we only did a maximum antibody coating density case for the 1 μm particles. The ELISA was performed using a horseradish peroxidase (HRP) conjugated anti-mouse k-light chain specific monoclonal antibody to characterize the particle surface antibody density for both micro/nano particles. The specificity of the reagent to mouse antibody light chains provided a direct measurement of the anti-ICAM-1 binding sites available on the particle. Particles were incubated with 5% HRP conjugated anti-mouse k-light chain specific monoclonal antibody for 30 min, followed by washing with 1% BSA solution and clearing out of unbound antibody through centrifugation. 50 μl of the particle solution were loaded on a 96-well plate, and the particle concentration was analyzed. Then, 50 μl of Amplex Ultra Red reagent was added to each well, and the reaction was allowed to proceed for 10 min at room temperature. The fluorescence intensity of the particle sample with Amplex Ultra Red reagent was observed on a microplate reader at 544 nm

TABLE I. Final particle concentration (#/ml) for 210 nm and 1 μm particles. The total particle volume is constant for both particles.

Particle size	Final particle concentration	Total particle volume (μm^3)
210 nm	4.77×10^9/ml	2×10^7
1 μm	3.85×10^7/ml	2×10^7

excitation/590 nm emission. The fluorescence intensities were converted to the number of HRP molecule using the calibration curves prepared using biotinylated-HRP conjugation as by Haun and Hammer[21] Assuming a 1:1 binding ratio between anti-ICAM-1 and secondary antibody, the anti-ICAM-1 density on the particles was determined. 210 nm and 1 μm particle antibody coating density based on fluorescence intensity was compared to estimate the relative accuracy of the technique. If steric hindrance does not prohibit κ-light chain antibody interaction on the second light chain, the estimate of concentration could be off by 2 fold.

Endothelial cell culture in the device

Primary bovine aortic endothelial cells (BAOECs) were cultured in the upper channel of the device as the endothelial cell layer model. Confluent monolayers of endothelial cells were adapted to physiological flow conditions, and effect of flow mediated localized action of TNF-α was examined. BAOECs were cultured in 4-(2-hydroxyethyl)-1-piperazineethanesulfonic acid (HEPES) buffered Dulbecco's modified eagle medium (DMEM) supplemented with 10% heat inactivated fetal bovine serum (Atlanta Biologicals, Inc.) and having a final concentration of 100 I.U./ml penicillin and 100 μg/ml streptomycin (Sigma-Aldrich). The device was sterilized in UV light overnight. Prior to cell seeding, the upper channel and the membrane of the device were coated with 50 μg/ml fibronectin solution (Sigma-Aldrich) overnight at 37 °C. The channel was rinsed with media to remove any excess, unattached fibronectin. BAOECs cells were seeded onto the semi-permeable membrane in the upper channel at a density of 2×10^7 cells/ml. Cell seeded devices were placed in an incubator under standard culture conditions (37 °C and 5% CO_2) overnight to allow cell attachment and spreading on the membrane. For the next 12 h, the upper channel of the device was subjected to flow based media change at low FSS (0.01 dyn/cm^2). Thus, a constant supply of fresh media was available for the BAOECs without being subjected to FSS effects. Later, the flow rate of media in the upper channel was gradually increased to subject the endothelial cells to physiologically relevant FSS values.

Application of fluid shear stress

Endothelial cells are exposed to continuous FSS *in vivo* which regulates signaling pathways that maintain their phenotype. This is critical to the success of our work, and for this the confluent layer of BAOECs was subjected to physiologically relevant FSS. To calculate the volumetric flow rate that correspond to the required maximum FSS experienced by the endothelial cells, the following equation was used,[22] where "τ_{cell}" is the maximum local shear stress experienced by endothelial cells, and "μ" is the fluid viscosity. "Q" is the volumetric flow rate through the region of interest, "w" is the width of the channel, and "h" is the distance between the top and bottom surface of the channel

$$\tau_{cell} = \frac{6\mu Q}{wh^2}.$$

On reaching confluence, the BAOECs were subjected to a FSS of 12 dyn/cm^2 using an extremely low pulsation peristaltic pump (ISMATEC, IPC-N series) placed in standard culture conditions. The use of a peristaltic pump allowed multiplex access to the flow channel, providing the flexibility of introducing new entities (particles, specific biomolecules, etc.) without disturbing the laminar FSS to which the BAOECs were subjected.

TNF-α treatment

After establishing the *in vitro* bio-mimetic blood vessel platform, the dynamics of endothelial activation and ICAM-1 expression by local action of TNF-α were studied. The occurrence of a pathological condition leads to upregulation of endothelial cell adhesion molecules. This process is mediated by circulating cytokines such as TNF-α. ICAM-1, a cell-surface glycoprotein member of the Ig super-family is expressed by normal vascular endothelium at a basal

level of surface density[23,24] that markedly increases under pathological conditions including inflammation as a result of endothelial activation.[23–25]

BAOECs were subjected to 24 h or more of flow at 12 dyn/cm^2 and were finally activated with TNF-α to study surface ICAM-1 expression. TNF-α was mixed in media at a concentration of 10 Units (U)/ml, and the treatment was performed for 2 h on a confluent endothelial cell layer (>80%). BAOECs were locally activated by introducing TNF-α in the lower channel of the device, which has direct access to a section of the upper channel. TNF-α diffused from the lower to the upper channel through the pores of the membrane and locally activated the endothelial layer from the basal side. The upper channel has been divided as "upstream," "TNF-α treated," and "downstream" sections with respect to the direction of media flow (Fig. 1), and TNF-α in the lower channel comes in direct contact with the endothelial cells in the "TNF-α treated" section of the upper channel. BAOECs in the upstream or downstream sections did not come in direct contact with the pro-inflammatory cytokine. Most likely, mass transfer of materials between the upper and lower channels is mediated by gradient-driven diffusion through the membrane pores, although, in theory, endothelial cells may exert active directional transport of specific compounds via enzymatic and energy-dependent mechanisms.

Anti-ICAM-1 coated particle binding on BAOEC layer

Antibody coated particle binding was performed on locally TNF-α activated BAOECs to characterize surface ICAM-1 expression. Anti-ICAM-1 coated probe particles were introduced to the flow in the upper channel, while localized TNF-α activation of endothelial cells was conducted from the lower channel. This allows the study of dynamics and heterogeneity involved in endothelial ICAM-1 upregulation induced by local action of TNF-α as close to native *in vivo* condition as possible.

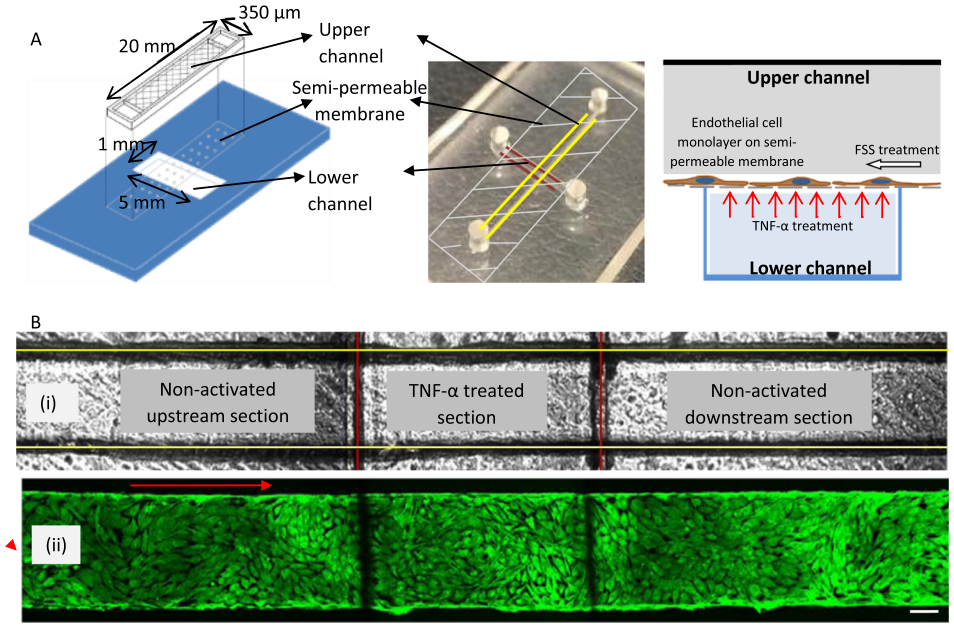

FIG. 1. (a) Graphical schematic (left) and photograph (center) of the bi-layer device showing the upper (marked with yellow lines) and lower (marked with red lines) channel separated by a semi-permeable membrane. The schematic on the right depicts the culture of a monolayer of endothelial cell on the semi-permeable membrane and the manner in which TNF-α treatment is performed from the lower channel. (b) (i) Bright field image of the upper (marked with yellow lines) and lower (marked with red lines) channel defining the upstream, TNF-α activated, and downstream sections. (ii) Fluorescently labeled F-actin cytoskeleton (FITC phalloidin) images of confluent BAOEC layer aligned to flow (12 dyn/cm^2 FSS for 24 h). The cells are cultured on the semi-permeable membrane in the upper channel of the device. Arrow shows flow direction (Scale bar: 100 μm).

Particle concentrations for 210 nm and 1 μm particles for performing the binding test were chosen such that the "total volume of particles" remained a constant (Table I). Also, the flow time for each flow case was reduced proportional to an increase in FSS to maintain the "total volume of particle solution" for all cases a constant (Table II). This made sure that the "total number of particles/flow case" remained the same for all flow cases.

The particles were introduced to the flow in the upper channel of the device, and after their designated flow time unbound particles were removed by flushing with a buffer solution. The wash buffer contains a plasma membrane stain (CellMask^{TM}, Life technologies) to fluorescently tag the BAOECs. The particle bound BAOECs were then fixed in paraformaldehyde (3.7%). Particle binding was analyzed by phase contrast and fluorescence microscopy (FV1000-IX81, Olympus), and image analysis was performed using ImageJ software.

Real time particle binding study

To demonstrate the applicability of our platform towards real time *in situ* studies, we characterized dynamic binding of anti-ICAM-1 coated NPs on BAOECs being activated by TNF-α. The enclosed nature of the blood vessel platform allowed maintenance of sterile conditions. We performed a continuous particle binding study over time where the flow set-up was assembled on a microscope table. BAOECs were subjected to 12 dyn/cm^2 of FSS for 6 h before being locally treated with TNF-α from the lower channel, while flow is continued in the upper channel. Real time binding of anti-ICAM-1 coated 210 nm particles (high density) was analyzed to characterize the dynamic nature of ICAM-1 expression by BAOECs. An illustration of the set-up is given in Fig. 8(a). The cells were cultured in HEPES buffered media, and such cultures do not require a controlled gaseous atmosphere.[26] The pump controlled the flow rate of the media, and an in-line solution heater (Warner Instruments, SH-27B) maintained the media temperature at 37 °C. The objective of the microscope was covered with a thin-film heating band (Bioptech, 150819) to facilitate live cell imaging as optical coupling medium (oil) can act as a thermal coupling medium and draw heat away from the microfluidic chip.

RESULTS AND DISCUSSION

On chip cell culture

Endothelial cells, which form the tunica intima, are constantly exposed to blood flow. The exposure of endothelial cells to this shear stress activates a number of cellular mechano-sensors and adaptor molecules that regulate the expression of genes and proteins relevant to endothelial cell functions in healthy and disease conditions.[27,28] Pro-inflammatory and proliferative signaling pathways of vascular endothelial cells become down-regulated when the endothelial cell layer is exposed to unidirectional sustained FSS.[29] Subjecting the endothelial cells to physiologically relevant FSS helps maintain their phenotype.[30] We validated the bio-mimetic nature and checked the longevity of cell culture in our device. A confluent layer of BAOECs was subjected to steady and directed laminar FSS (12 dyn/cm^2) for a time period of 5 days. A confluent and flow-aligned BAOEC monolayer was maintained for 5 days, and the F-actin arrangement pattern was comparable to that of BAOECs subjected to 12 dyn/cm^2 FSS for 24 h [Fig. 2(b)].

TABLE II. FSS and corresponding volumetric flow rate values along with flow time for 6, 12, and 18 dyn/cm^2 cases. Flow time decreases with FSS to maintain the "total volume of particle solution/flow case" a constant.

Flow shear stress (dyn/cm^2)	Flow rate in ml/h (viscosity: 0.007 dyn s/cm^2 for media)	Flow time (minutes) for particle flow study in media/pure buffer
6	1.8	6
12	3.6	4
18	5.4	2

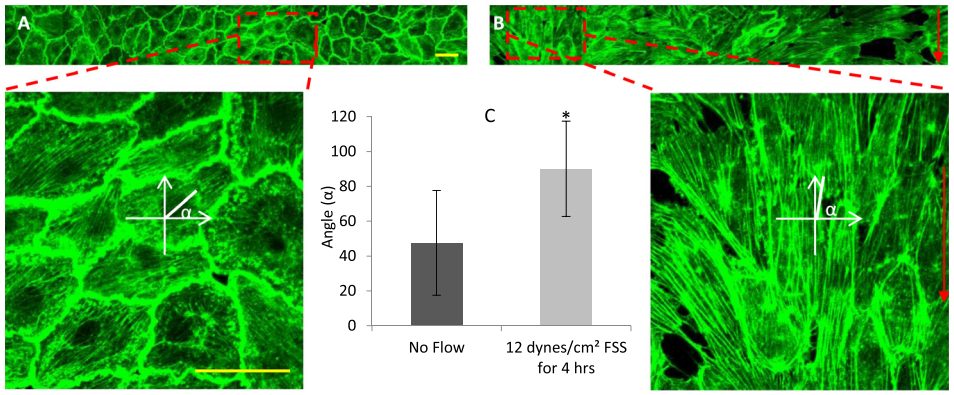

FIG. 2. Organization of F-actin stress fibers (green) in BAOECs assessed by confocal microscopy (a) static case; cell stress fibers tend to align parallel to the width of the channel. (b) After 4 h of flow at 12 dyn/cm^2 FSS; cell stress fibers tend to align parallel to the flow direction (scale bar: 50 μm). Insets show zoomed in images of stress fiber alignment. Arrows (red) mark the flow direction. (c) Quantitative measurement of stress fiber alignment angle (α) to the width of the channel under static and flow shear stress case. Data are shown as mean ± S.D. (n = 50 cells from 3 independent experiments) (*p < 0.001 by Student's *t*-test).

BAOEC stress fiber alignment under FSS

To further examine the endothelial cell layer subjected to flow, their actin assembly characteristics were studied. Endothelial cells exposed to FSS change shape and microfilament network to align with the direction of flow.[31] We examined this by staining F-actin stress fibers of BAOECs growing in the upper channel. The exposure of cells to 12 dyn/cm^2 FSS resulted in alteration of cell shape from the typical cobblestone pattern to fusiform as observed in endothelial cells *in vivo*.[32,33] Majority of the cells and their actin stress fibers form a series of almost parallel fibers in the long axis of the cell, aligned in the direction of flow (Fig. 2(b)). The control (no flow) case had the cortical actin, and F-actin fibers arranged in a radial pattern (Fig. 2(a)). To better depict the relationship between cell orientation and flow direction, the angle (α) between the orientation of stress fibers and the width (short-axis) of the microchannel was plotted using ImageJ software. It is observed that for the control case the stress fibers align at an average angle of 51.4°, while the cells exposed to flow show an average angle of 90.1° (Fig. 2(c)). This result is consistent with previous studies.[31,34]

When exposed to FSS, the redistribution of cortical actin from the periphery of the endothelial cell to bundles of stress fibers aligned in the direction of flow is expected.[35–38] The thickness of the cortical actin and width of stress fibers were calculated based on the analysis of fluorescence labeled actin cytoskeleton images. In BAOECs subjected to 12 dyn/cm^2 of FSS for 4 h, the thick cortical actin was found to reorganize into actin stress fibers along the direction of flow (Fig. 3). About 2 fold decrease in cortical actin thickness is observed (Fig. 3(a)). The apparent thickness of stress fibers increases around 2 fold as well for BAOECs subjected to FSS (Fig. 3(b)).

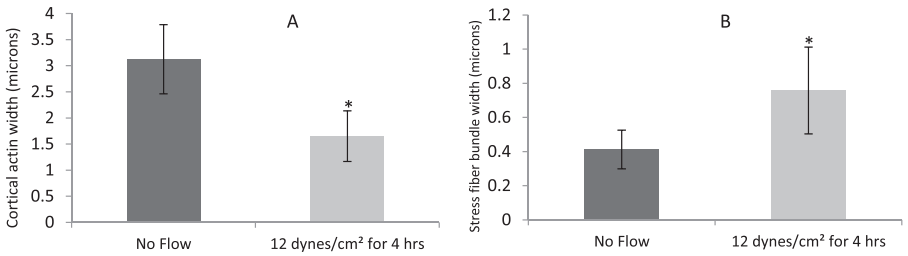

FIG. 3. Reorganization of cortical actin into stress fiber bundles in BAOECs subjected to FSS. Flow-induced actin remodeling was observed by fluorescence labeling of the actin cytoskeleton with FITC-conjugated phalloidin in BAOECs treated with 12 dyn/cm^2 FSS for 4 h. Comparison of (a) cortical actin thickness and (b) stress fiber bundle width distribution in static and flow (12 dyn/cm^2 FSS for 4 h) culture conditions. Data are shown as mean ± S.D. (n = 50 cells from 3 independent experiments). (* p < 0.001 by Student's *t*-test).

Since the actual thickness and the density of the stress fibers formed cannot be understood from analyzing the width of the stress fibers alone (stress fiber bundle depth in the z direction is not considered), we quantified their fluorescence intensity in grayscale value and plotted the corresponding line graphs (Figs. 4(a) and 4(b)). This also gives an idea of the stress fiber density present in each cell. The exposure of endothelial cells to FSS results in assembly of thick stress fibers along the direction of flow.[39] We observed multiple but less intense stress fiber distribution across the cytoplasm of static BAOECs [Figs. 4(a-i) and 4(a-ii)]. BAOECs subjected to flow have fewer but more profound and sharp stress fiber distribution [Figs. 4(a-iii) and 4(a-iv)]. Stress fiber density in the cells was quantified through a line profile across the cytoplasm of BAOECs and using ImageJ software to calculate fluorescence intensity.[40] The software identifies the stress fibers by their increased fluorescence relative to areas devoid of stress fibers. Sharp, distinct peaks represented individual stress fibers, while the width and the fluorescence intensity of the peak indicated their thickness [Fig. 4(b-i)]. Actin stress fibers were quantified as thin and thick for both static and FSS case by classifying stress fibers based on their fluorescence intensity

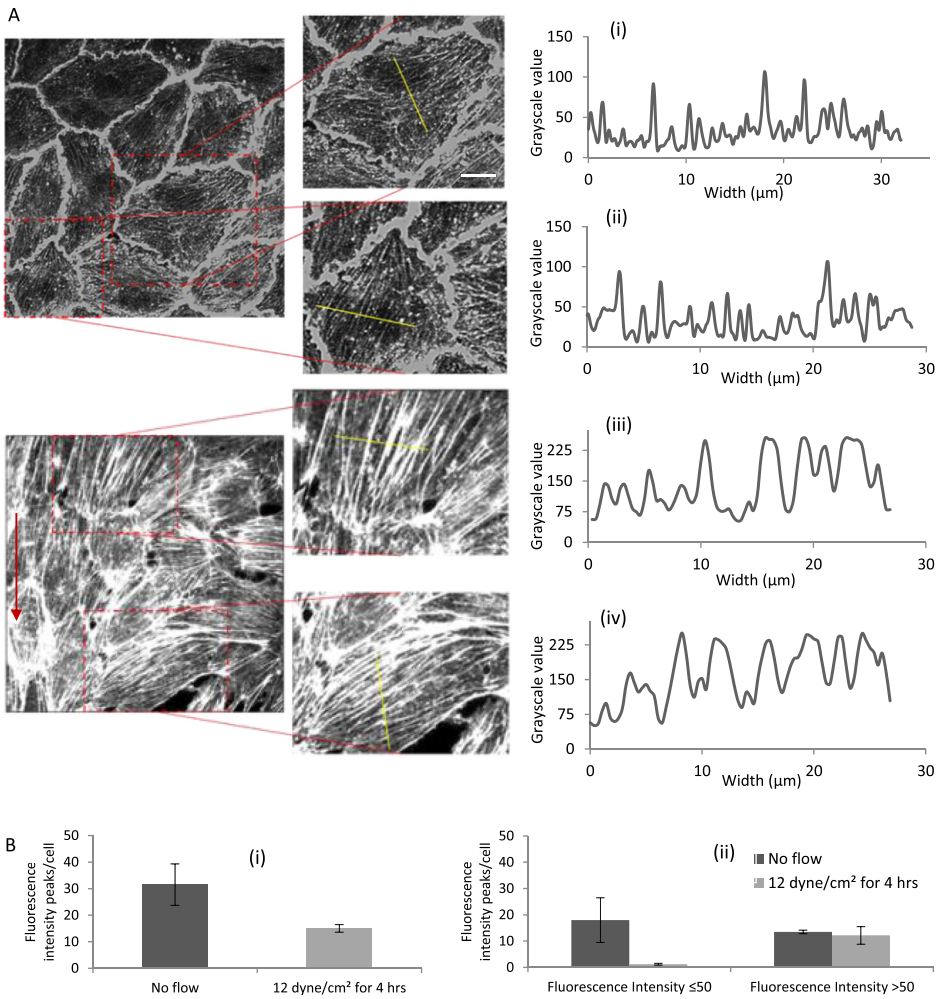

FIG. 4. Comparison of stress fiber distribution in BAOECs subjected to FSS with no flow case. Actin stress fibers of BAOECs are labeled with FITC-conjugated phalloidin. (a) Fluorescence intensity (grayscale value) of stress fibers is quantified using ImageJ software across the marked line and corresponding line graphs are plotted for: (i) and (ii) No flow case (control); and (iii) and (iv) endothelial cells subjected to FSS at 12 dyn/cm^2 for 4 h. (b) (i) Total number of fluorescence intensity (grayscale value) peaks denoting stress fiber bundles in control and flow case. (ii) Thin and thick actin stress fiber bundles in BAOECs were marked by classifying them based on grayscale value ($\leq$50 as thin and >50 as thick) for both control and FSS case. Arrow indicates direction of flow. (Scale bar: 10 μm). Data are shown as mean $\pm$ S.D. (n = 50 cells from 3 independent experiments).

(grayscale value). For statistical purpose, the stress fibers with fluorescence intensity ≤50 grayscale value were arbitrarily marked as thin and >50 as thick [Fig. 4(b-ii)]. There was almost an equal distribution of thin and thick stress fibers in static cells, while the BAOECs subjected to FSS had a significant distribution of thick stress fibers in their cytoplasm. Laminar and sustained FSS induces thicker stress fiber organization of endothelial cells along the direction of flow, while maintaining elongated cell morphology.

Characterization of flow-mediated localized BAOEC activation using fluorescent probes

TNF-α activated BAOECs would have upregulated expression of ICAM-1 among other endothelial cell surface proteins.[41] A time course study on TNF-α based expression of surface ICAM-1 by BAOECs cultured in petri-dish showed 2 h of treatment to be optimal (Fig. 5(b-iii)). The BAOECs are cytokine-treated from the basal side of the cell, and to understand the difference in basal and apical cell side TNF-α treatment on surface ICAM-1 expression BAOECs were subjected to these two cases separately. The cells expressed similar levels of ICAM-1 expression for both cases characterized by targeted particle binding (supplementary material Figure 1).[42] In our work, the ICAM-1 expression was evaluated by studying specific binding of anti-ICAM-1 coated particles to endothelial cells in the upper channel (Fig. 5(b)). Similar particle based probes have been used in other studies to understand ICAM-1 dynamics associated with transendothelial

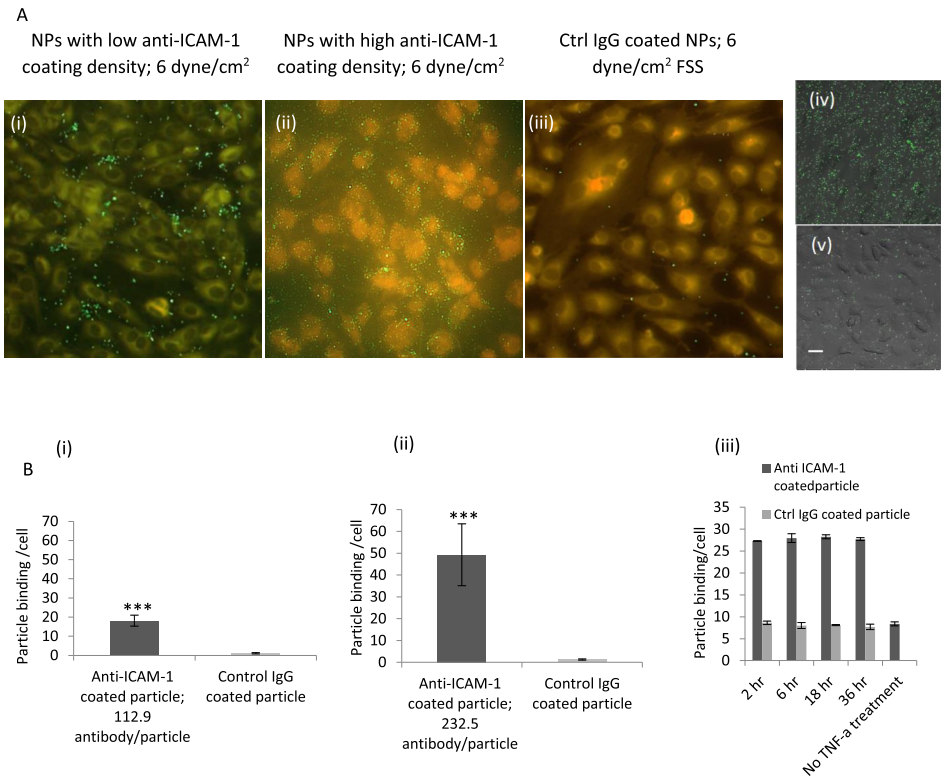

FIG. 5. (a) Fluorescence micrographs show binding of 210 nm particles under flow on TNF-α activated endothelial cells for 2 h, (i) anti-ICAM-1 coated NP (low density case) at FSS of 6 dyn/cm^2; (ii) anti-ICAM-1 coated NP (high density case) at FSS of 6 dyn/cm^2; and (iii) control IgG coated NP at FSS of 6 dyn/cm^2. (Scale bar: 20 μm). Fluorescence micrographs show binding of 210 nm particles on TNF-α activated endothelial cells for 2 h in a static petri-dish study (iv) anti-ICAM-1 coated NP (high density case) and (v) control IgG coated NP; (scale bar: 20 μm). (b) Quantification of anti-ICAM-1 and control IgG coated NP binding per cell at a FSS of 6 dyn/cm^2 on TNF-α activated endothelial cells for 2 h, (i) low density anti-ICAM-1 coated NP; and (ii) high density anti-ICAM-1 coated NP. Endothelial cells were subjected to 24 h or longer of flow at 12 dyn/cm^2 and were activated with TNF-α. Then, antibody coated particles were flown according to parameters listed in Table II. (iii) Quantification of anti-ICAM-1 (high density case) and control IgG coated 210 nm particles binding per cell on endothelial cells TNF-α activated for different time points for the static petri-dish study. Data are shown as mean ± S.D. (n = 100 cells from three independent experiment for each case). (*** $p < 0.00001$ by Student's *t*-test).

leukocyte migration[43] and inflammatory responses.[44] Saturated anti-ICAM-1 coating on 210 nm particles produced a high antibody coating density of 232.5 ± 25 anti-ICAM-1/particle. This was brought down to a low antibody coating density of 112.9 ± 19 anti-ICAM-1/particle using control IgG antibody. These correspond to $1851.2 \pm 199/\mu m^2$ for the maximum antibody density case and 898.9 ± 151 anti-ICAM-1/μm^2, respectively, and would be referred to as high and low density cases from now. 1 μm particles had a single antibody density case of 2367.8 ± 264 anti-ICAM-1/particle, which corresponds to 232.9 ± 25 anti-ICAM-1/μm^2. 210 nm particles coated with anti-ICAM-1 or control IgG were perfused at 6 dyn/cm^2 FSS. Anti-ICAM-1 coated NP bound to cytokine-activated endothelial cell specifically, exceeded binding of control IgG coated NP by ~20 times and ~50 times for the low and high density anti-ICAM particle coating cases, respectively ($p < 0.00001$) (Fig. 5(a)). Anti-ICAM-1 coated NP binding to TNF-α treated EC was further enhanced in FSS-exposed vs static endothelial cells, consistent with observations in other models[45] (Fig. 5(b-ii) vs 5(b-iii)).

Tsou *et al*. investigated the endothelial spatial regulation of adhesion molecules on a linear gradient of FSS from 0 to 16 dyn/cm^2 on a Hele-Shaw flow chamber design.[13] Even though membrane based devices have been used before for endothelial cell culture studies,[4,46] the spatial variation in inflammatory response based on cytokine triggering has not been studied. The design of our bio-mimetic blood vessel platform allows a section of the upper channel to be accessed independently. This facilitates spatially controlled cytokine activation of endothelial cells. Having both direct cytokine-activated and non-activated endothelial cells in the same channel allowed investigation of the heterogeneous nature of ICAM-1 expression and the hemodynamic control of the marginal zone between inflammation foci and relatively normal vasculature. Investigating the binding of anti-ICAM-1 coated particles of different size and antibody coating densities to ICAM-1 under physiologically relevant FSS characterizes the distribution and accessibility of ICAM-1 on endothelial cells. Such studies can shed light on parameters involved in receptor-ligand recognition for activated blood cells and affinity drug carriers.

Endothelial cells were subjected to 24 h or more of flow at 12 dyn/cm^2 and were activated with TNF-α from the lower channel at a concentration of 10 Units (U)/ml. Once activated, anti-ICAM-1 coated particles were flown according to parameters mentioned in Table II. As the endothelial cells were fluorescently tagged, the boundaries of individual cells were marked, and the number of particles binding per cell was counted using ImageJ software. The binding of fluorescent particles to ICAM-1 in the upstream, TNF-α treated, and downstream areas of the channel was studied using antibody coated 210 nm and 1 μm particles. Flow rates of 6, 12, and 18 dyn/cm^2 were employed after the BAOECs were treated with TNF-α for 2 h under a steady and sustained FSS of 12 dyn/cm^2.

From Fig. 6(b), it is observed that BAOECs in the TNF-α treated section of the upper channel have around 4–5 times higher particle binding density compared to the upstream section for 210 nm particle with high anti-ICAM-1 coating density ($p < 0.01$). A similar trend was observed for the lower antibody coating density case (Fig. 6(a)), and this was consistent for all the flow cases for both particle antibody coating densities. This clearly showed a significant increase in surface ICAM-1 expression in BAOECs at the TNF-α treated section. The p value is <0.01 by one way analysis of variance (ANOVA) test for particle binding data compared between TNF-α treated, upstream, and downstream regions for both 210 nm particle antibody coating density cases. The downstream section of the channel also showed significantly higher (around 2 times) particle binding density compared to the upstream section ($p < 0.01$). TNF-α induced increase in endothelial ICAM-1 expression has been well established.[47] A study on their spatial regulation based on localized cytokine treatment is novel and has been detailed in the section on ICAM-1 and F-actin distribution along the channel length. From our particle probe binding based analysis of surface ICAM-1 expression, FSS exposed endothelial cells (Figure 5(b-ii)) are found to have around two times higher ICAM-1 expression compared to static case (Figure 5(b-iii)). Although in the static case the probes are also statically incubated on the activated endothelium rather than subjected to flow based binding, this variance is being overlooked in this comparison. Similar increase in TNF-α induced expression of surface ICAM-1 on shear exposed endothelial cells when compared to static cultured cases have been

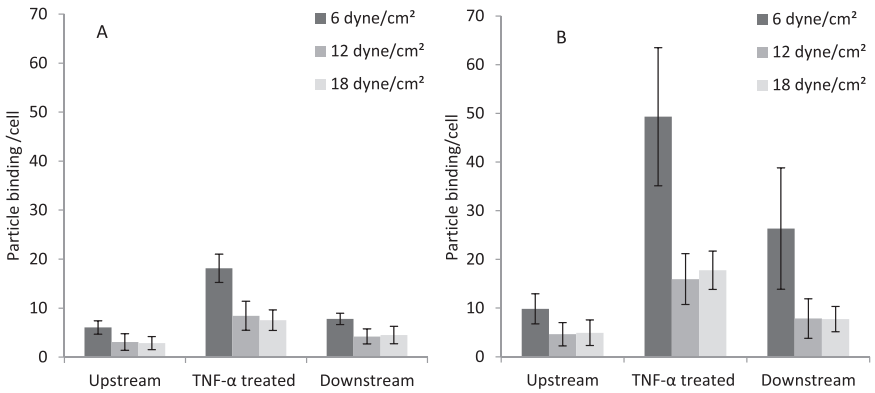

FIG. 6. Targeted binding of anti-ICAM-1 coated particles of different antibody coating densities on BAOECs in the upstream, TNF-α treated, and downstream sections of the channel at different shear rates. Quantification of particle binding density per cell at 6, 12, and 18 dyn/cm^2 for 210 nm particles of (a) low anti-ICAM-1 coating density and (b) high anti-ICAM-1 coating density. $p < 0.01$ by one way ANOVA test for particle binding data compared between upstream, TNF-α treated, and downstream regions for both low and high density anti-ICAM-1 particle coating cases. Data are shown as mean ± S.D. (n = 100 cells from three independent experiments for each case).

previously reported. Chiu *et al*. observed an increase in surface ICAM-1 expression using flow cytometry based analysis on human umbilical vein endothelial cells (HUVECs), while Klingberg *et al*. found shear adapted and TNF-α treated HUVECs to have higher binding with anti-ICAM-1 coated NPs compared to static case.[45]

The particle binding density depends on the antibody coating density as well. When compared to the high particle antibody coating density case, the particle binding density was around half for the low case. This increased binding density of particles with higher antibody coating is consistent with other studies and our previous work.[21,48,49] Previous studies have reported the binding kinetics of particles with higher anti-ICAM-1 coating density to be significantly faster,[48,50] which could be valid for our study as our maximum particle flow time is only 6 min. The particle binding density decreased when the FSS increased from 6 to 12 dyn/cm^2 for both anti-ICAM-1 coating density cases. An increase in FSS reduced the available time for particles to diffuse/marginate towards the endothelial cell surface, which reduced their binding density as observed in other studies.[48] The particle binding density also does not reduce for FSS > 12 dyn/cm^2 (Fig. 6). Similar behavior has been reported in previous studies where it is observed that flow cannot generate enough drag force on the particle to significantly reduce the particle binding density after a critical shear rate.[48] Here, the receptor-ligand bond strength between the 210 nm particle and the ICAM-1 molecules expressed on the endothelial layer should be higher than the drag force produced by the FSS on the nanometer scale particle (drag force generated is proportional to the size of the particle).

Binding of anti-ICAM-1 coated 1 μm particles was also studied, but no significant binding was observed in any sections of the channel for a FSS range of 6–18 dyn/cm^2. Particle binding characteristics similar to that of 210 nm ones were observed when the FSS was brought down to 1.5 dyn/cm^2 (supplementary material Figure 2).[42] Drag force generated on the bigger 1 μm particle is higher, making them easily detachable. As described by Charoenphol *et al.,* there is a critical wall shear rate beyond which the higher disruptive hemodynamic force interferes with particle binding.[51] For 1 μm particle, 6–18 dyn/cm^2 could be beyond the critical shear rate. In addition, the role of accessibility and surface congruency of ICAM-1 is more limiting for large vs small ligand-coated particles.

ICAM-1 and F-actin distribution along the channel length

In order to study the transition in ICAM-1 expression in the different sections (upstream, TNF-α treated, and downstream) of the channel, we divided these sections into smaller segments and inspected the particle binding per cell along the length of the channel (Fig. 7(b)). An

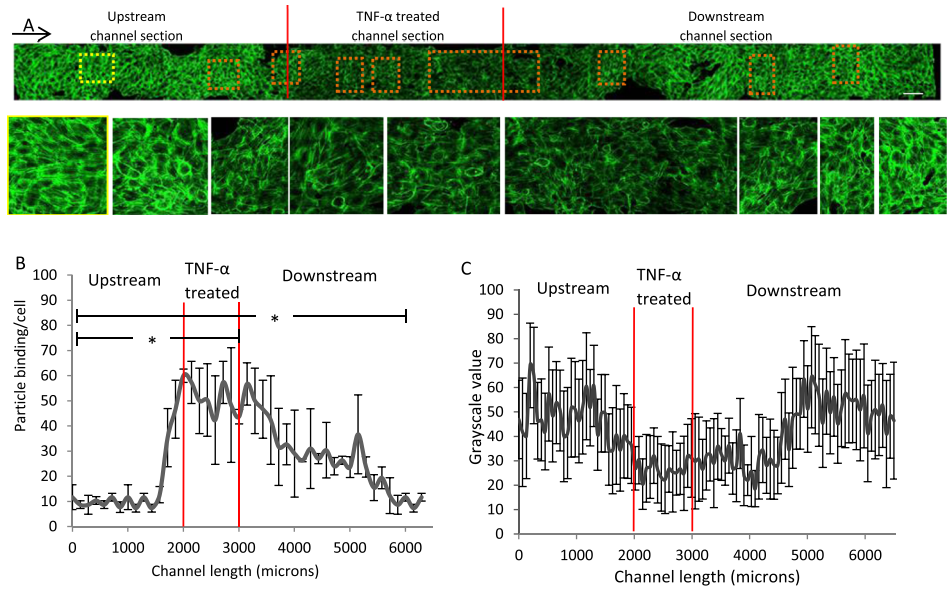

FIG. 7. Analysis of particle binding and F-actin stress fiber arrangement along the length of the channel after TNF-α treatment. (a) F-actin stained image of BAOECs aligned to FSS at 12 dyn/cm^2 for 4 h and TNF-α treated (10 U/ml) for 2 h. Zoomed in image (corresponding to dashed boxes) shows more clear F-actin arrangement. Yellow bordered image represents control BAOECs flow aligned to 12 dyn/cm^2 FSS. Magnified images (3.5× magnification) are arranged in the same order as the dashed boxes in the intact image above. (b) 210 nm anti-ICAM-1 (high density) coated particle binding per cell at 6 dyn/cm^2 FSS along the length of the channel divided into upstream, TNF-α treated, and downstream sections (*$p < 0.01$ by Student's *t*-test for particle binding data compared between "upstream-TNF-α treated" and "upstream-downstream" sections.) (c) Fluorescence intensity (grayscale value) of stress fibers is quantified using ImageJ software across the length of the channel and corresponding graph is plotted. Data are shown as mean ± S.D. Arrow indicates flow direction. (Scale bar: 100 μm). Data are shown as mean ± S.D. (n = three independent experiment for each case).

increase in binding/cell for anti-ICAM-1 coated particles (high density) as a result of increased ICAM-1 expression by endothelial cells was observed all along the 1 mm long TNF-α treated section. This also extended into the nearby downstream section. Particle binding density in the downstream section was significantly higher than that of the upstream section, even though both sections were not TNF-α treated directly. There was a smooth decrease in particle binding along the channel in the downstream section, and after a channel length of about 3 mm the particle binding density became comparable to that of upstream region. The significance of the difference in particle binding densities between the "upstream-TNF-α treated" and "upstream-downstream" sections of the channel was evaluated using Student's *t*-test, and the p value was found to be <0.01. Elevated particle binding density was also observed in the upstream section of the channel close to the TNF-α treated section (red lines mark the boundary in Figs. 7(a) and 7(b)). TNF-α treatment leads to cell-cell barrier dysfunction and intercellular gap formation in endothelial cells, thus increasing blood vessel permeability.[52–54] The increase in particle binding in the upstream section close to the TNF-α treated section and along the length of the downstream section could be due to a synergistic influence of flow and TNF-α diffusion through the BAOEC layer which has increased permeability in the TNF-α treated region. Flow directed from the TNF-α treated to the downstream section carried a majority of the diffused TNF-α molecules towards the downstream section. The exposure to TNF-α led to upregulation of ICAM-1 expression on BAOECs here, which decayed along the channel length as the distance from direct TNF-α exposure increased and endothelial cells in its path bound remaining TNF-α.

Inflammatory conditions lead to rearrangement of the actin cytoskeleton at endothelial cell junctions, regulation of endothelial permeability, and barrier modulation.[55–58] We looked into F-actin stress fiber arrangement after TNF-α treatment along the channel length to further understand the endothelial cell microenvironment (Fig. 7(a)). A confluent BAOEC layer was exposed to 4 h of FSS at 12 dyn/cm^2, which was followed by 2 h of localized TNF-α treatment

(10 U/ml) from the lower channel. The cells were stained for F-actin stress fibers, and their arrangement was studied in the upstream, TNF-α treated, and downstream sections. BAOECs exposed to FSS in the upstream section had stress fibers aligned to flow direction (yellow bordered image in Fig. 7(a)) as observed earlier (Fig. 2(b)). After 2 h exposure to TNF-α, there was thinning of stress fiber filaments around the center of the cell cytoplasm. Fig. 7(c) quantifies the fluorescence intensity (grayscale value) of F-actin stained stress fibers in the cell across the channel length using ImageJ software. The thinning started around the border of upstream and TNF-α treated section. It was consistently observed all throughout the TNF-α treated section and continued towards the downstream section. We observe an average drop of about 50% in the grayscale value of the fluorescence intensity in these sections (Fig. 7(c)). The F-actin stress fiber fluorescence intensity in the cell center increased smoothly to levels comparable to the upstream section after about 1.5 mm length in the downstream section. The thinning in F-actin fibers was likely due to TNF-α induced F-actin remodeling observed in endothelial cells.[52] Along the channel length, a rearrangement in F-actin stress fibers is also observed in BAOECs after TNF-α treatment. These isolated disruptions of the F-actin lattice were sparsely observed in the upstream regions close to TNF-α treated section, while they were more common in the TNF-α treated section. This was observed in the downstream section as well but the frequency of occurrence decreased along the channel length. This rearrangement of F-actin is a good indicator of barrier dysfunction and intercellular gap formation as a result of TNF-α treatment.[52–54] There is evidence of Cdc42, Rac, and Rho activation in a hierarchical cascade following stimulation with TNF-α in endothelial cells, leading to actomyosin-mediated cell retraction and formation of intercellular gaps.[59] Formation of intercellular gaps and barrier dysfunction would lead to TNF-α diffusion to the upper channel from the lower channel in our device, which is consistent with our assumption.

Dynamic nature of surface ICAM-1 expression by BAOECs

The blood vessel microfluidic model has a closed design, and this allows the maintenance of cell culture conditions inside the channel to sustain cell growth outside an incubator. By mounting the required experimental set-up on a microscope table (Fig. 8(a)), real time *in situ* studies can be performed on our blood vessel model. We applied this to study the dynamics of

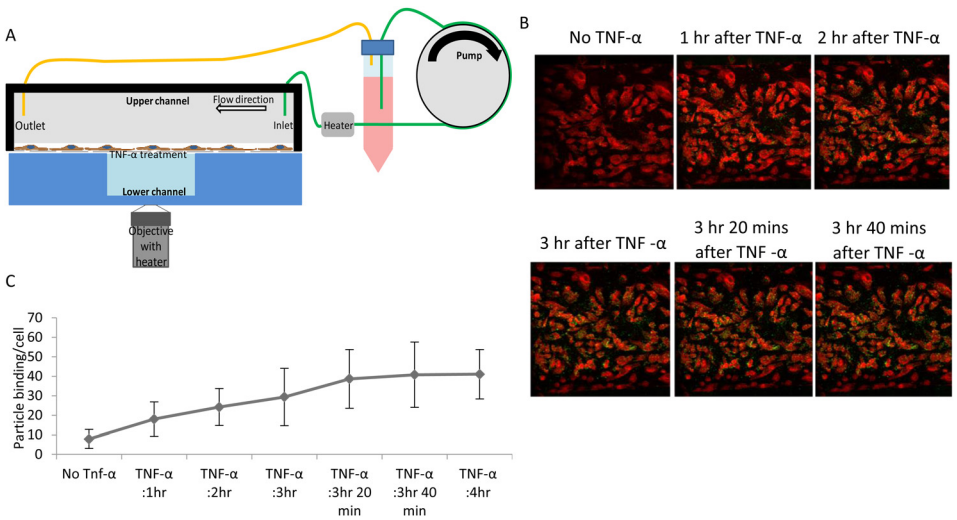

FIG. 8. (a) Schematic describing the experimental set-up for real time *in situ* particle binding study using the biomimetic blood vessel platform. (b) Images of 210 nm (green fluorescence) particle binding over red fluorescence plasma membrane stained (CellMask, Life technologies) cells for different TNF-α treatment time points. BAOECs were subjected to 12 dyn/cm^2 of FSS for 6 h before localized TNF-α treatment. (c) Anti-ICAM-1 coated (high density) 210 nm particle binding data over time are plotted to characterize the dynamic nature of surface ICAM-1 expression by BAOECs before and after TNF-α treatment. (n = three independent experiment).

endothelial surface ICAM-1 expression induced by flow mediated TNF-α activation. The dynamics were characterized by studying the specific binding of 210 nm fluorescent anti-ICAM-1 coated particles (high antibody coating density) on BAOECs activated locally with TNF-α. The device with a monolayer of flow aligned endothelial cells in the upper channel was mounted on the microscope table and subjected to a FSS of 12 dyn/cm^2 for 6 h before being locally TNF-α treated from the lower channel for 4 h. Anti-ICAM-1 coated particles were introduced to the flow, and images were taken every 20 min to analyze the increase in particle binding on cell surface. The particle binding density per cell increased, corresponding to an upregulation of ICAM-1 expression by BAOECs. This study provides a better understanding of the dynamics of ICAM-1 upregulation by BAOECs over time. Unlike that observed in static petri-dish studies where the ICAM-1 upregulation peaked after 2 h (supplementary material Fig. 1), this *in situ* observation under FSS showed a linear increase in ICAM-1 upregulation which peaked after 3 h and 20 min (Fig. 8(c)). The increased ICAM-1 expression in this case was a combined effect of flow and cytokine activation, as one could expect *in vivo*. This study provides a better understanding of the transient nature of ICAM-1 receptor upregulation by BAOECs when locally activated by TNF-α in a flow-mediated realistic environment. As explained earlier, flow adapted endothelial cells produce more surface ICAM-1 expression compared to static case when triggered with TNF-α.[45] An integrated effect of shear stress along with TNF-α is observed here, comparable to similar effect reported in the work by Srigunapalan *et al.* where monocyte adhesion increased when stimulated with shear stress and TNF-α.[46]

CONCLUSION

In designing *in vitro* models of human pathophysiology, one needs to critically define which specific parameters and biological mechanisms typical for the condition of interest it may and may not adequately address. For example, the range of flow shear stress explored in this study is typical of microvasculature and small veins. Therefore, it would be inadequate for studies of interactions of blood with endothelium in arterial lumen, which is an important site of atherosclerosis and thrombosis. This range of shear stress fits better with hydrodynamic conditions in other types of inflammation such as acute lung injury or acute respiratory distress syndrome. Furthermore, these conditions seem to be relevant to vasa vasorum, which represent specific and important site of endothelial events in atherosclerosis and other pathological conditions in large arteries. Some parameters of *in vitro* models, such as concentration of biological mediators, are difficult to relate to their *in vivo* counterparts. For example, kinetics and amplitude of blood level of cytokines in humans and animal models differ, as do biological activities and interactions endogenous vs exogenous cytokines with various other molecular and cellular constituents in the body. In this context, concentration of TNF-α employed in the present study should be viewed as a conventional range used in *in vitro* models, rather than a reference to the pathological level of endogenous cytokine. In this study, we employed ICAM-1 targeted particles as a probe of the endothelial response. These probes help quantify the localized cytokine stimulation based ICAM-1 expression in a novel cell culture model, which allows comparison of endothelial cells upstream and downstream from the focal cytokine challenged site. The kinetics data for binding of ICAM-1 targeted particles show that our detection probe is reliable in a reasonable time frame.

We characterized BAOEC culture under physiological levels of flow and analyzed their F-actin organization pattern. Localized TNF-α treatment was performed on the BAOECs from the basal side, and flow mediated ICAM-1 upregulation was analyzed. Fluorescent antibody coated particle based imaging probes were utilized to characterize ICAM-1 expression on the endothelial cell layer by studying targeted particle binding under flow. By analyzing the particle binding along the length of the channel, we characterized the nature of upregulation and fall in ICAM-1 expression for BAOECs from the upstream to TNF-α treated and downstream channel sections. We also outlined the nature of TNF-α based F-actin remodeling and rearrangement along the channel length. By performing real-time particle binding study on this platform, the dynamics of TNF-α based ICAM-1 upregulation were also characterized. The blood vessel

model in this study is a tool with potential to characterize the complex microenvironmental heterogeneity of endothelial cells during inflammation and other pathologically significant states. This novel microfluidic chip can mimic closely the native environment of endothelial cells by facilitating *in vivo* levels of flow and biomolecule supply, along with an opening for localized access. It was found that the BAOECs in the TNF-α treated section of the channel exhibit upregulated ICAM-1 expression compared to the upstream and downstream section, while this device provided evidence that the BAOECs in the downstream section express higher ICAM-1 compared to the upstream section of the channel. Real-time particle binding studies on TNF-α activated BAOECs using this device revealed that the flow-mediated cytokine response by the endothelial cell layer is different from conventional static cases. This work highlights the versatile nature and functionality of the microfluidic biomimetic blood vessel platform developed. In comparison to *in vivo* systems, our work includes only a sub-endothelial compartment comprising of a monolayer of endothelial cells. Our future *in vitro* blood vessel models will incorporate the appropriate support cell systems (smooth muscle cells/pericyte) and extracellular matrix scaffold to answer relevant questions in vascular biology. This will take the model a step closer towards *in vivo* systems and extend its significance.

In this study, we detected appearance of ICAM-1 on the luminal surface of endothelium as a molecular marker. This parameter, widely used in the literature[49,60–62] as a conventionally accepted readout of functional status of these cells, is one of many manifestations of pro-inflammatory endothelial activation. They include cellular contraction and other surface alterations such as reduction of surface density of thrombomodulin, endothelial protein C receptor, and angiotensin-converting enzyme, as well as appearance of tissue factor, selectins, Willebrand factor, and other pro-coagulant and pro-inflammatory molecules. Each of these molecular changes is usually associated with specific functional changes including vascular adhesion of leukocytes, platelets, and fibrin. Accordingly, we envision further extension of our model in two intertwined directions. First, we will expand the list of molecular readouts of endothelial functional status using the current experimental setting. Second, we will embark on the analyses of pathophysiological consequences of these functional changes, including leukocyte adhesion and thrombosis, which will require adding blood or blood components to the perfusion system and corresponding modifications of the experimental setting.

ACKNOWLEDGMENTS

The authors acknowledge the support of this work from National Science Foundation (NSF) CAREER Grant Nos. CBET-1113040, NSF CBET-1067502, and National Institutes of Health (NIH) Grant No. EB015105.

The authors would like to thank Colin Orr, Sara Lynn Nicole Farwell, and Ming-Tzo Wei for research assistance, and Sara Lynn Nicole Farwell for critical manuscript review. Research from the Liu laboratory present herein was initiated with support from the Biosystems Dynamics Summer Institute, funded through an HHMI undergraduate education grant to Lehigh University.

[1]V. R. Muzykantov, "Targeted drug delivery to endothelial adhesion molecules," ISRN Vasc. Med. **2013**, 27.
[2]C. A. Staton *et al.*, "Current methods for assaying angiogenesis *in vitro* and *in vivo*," Int. J. Exp. Pathol. **85**(5), 233–248 (2004).
[3]L. L. Bischel *et al.*, "Tubeless microfluidic angiogenesis assay with three-dimensional endothelial-lined microvessels," Biomaterials **34**(5), 1471–1477 (2013).
[4]Y. Kim *et al.*, "Probing nanoparticle translocation across the permeable endothelium in experimental atherosclerosis," Proc. Natl. Acad. Sci. **111**(3), 1078–1083 (2014).
[5]Y. Zheng *et al.*, "*In vitro* microvessels for the study of angiogenesis and thrombosis," Proc. Natl. Acad. Sci. **109**(24), 9342–9347 (2012).
[6]D.-H. T. Nguyen *et al.*, "Biomimetic model to reconstitute angiogenic sprouting morphogenesis *in vitro*," Proc. Natl. Acad. Sci. **110**(17), 6712–6717 (2013).
[7]J. Borenstein *et al.*, "Functional endothelialized microvascular networks with circular cross-sections in a tissue culture substrate," Biomed. Microdevices **12**(1), 71–79 (2010).
[8]M. Tsai *et al.*, "*In vitro* modeling of the microvascular occlusion and thrombosis that occur in hematologic diseases using microfluidic technology," J. Clin. Invest. **122**(1), 408–418 (2012).
[9]M. Sato *et al.*, "Microcirculation-on-a-chip: A microfluidic platform for assaying blood- and lymphatic-vessel permeability," PLoS One **10**(9), e0137301 (2015).

[10]S. Kim *et al.*, "Engineering of functional, perfusable 3D microvascular networks on a chip," Lab Chip **13**(8), 1489–1500 (2013).
[11]I. K. Zervantonakis *et al.*, "Three-dimensional microfluidic model for tumor cell intravasation and endothelial barrier function," Proc. Natl. Acad. Sci. U.S.A. **109**(34), 13515–13520 (2012).
[12]V. van Duinen *et al.*, "Microfluidic 3D cell culture: From tools to tissue models," Curr. Opin. Biotechnol. **35**, 118–126 (2015).
[13]J. K. Tsou *et al.*, "Spatial regulation of inflammation by human aortic endothelial cells in a linear gradient of shear stress," Microcirculation **15**(4), 311–323 (2008).
[14]J. Rosano *et al.*, "A physiologically realistic *in vitro* model of microvascular networks," Biomed. Microdevices **11**(5), 1051–1057 (2009).
[15]N. Tousi *et al.*, "Preferential adhesion of leukocytes near bifurcations is endothelium independent," Microvasc. Res. **80**(3), 384–388 (2010).
[16]B.-H. Chueh *et al.*, "Leakage-free bonding of porous membranes into layered microfluidic array systems," Anal. Chem. **79**(9), 3504–3508 (2007).
[17]E. W. K. Young *et al.*, "Technique for real-time measurements of endothelial permeability in a microfluidic membrane chip using laser-induced fluorescence detection," Anal. Chem. **82**(3), 808–816 (2010).
[18]D. Huh *et al.*, "Acoustically detectable cellular-level lung injury induced by fluid mechanical stresses in microfluidic airway systems," Proc. Natl. Acad. Sci. **104**(48), 18886–18891 (2007).
[19]D. T. Eddington, J. P. Puccinelli, and D. J. Beebe, "Thermal aging and reduced hydrophobic recovery of polydimethylsiloxane," Sens. Actuators, B **114**(1), 170–172 (2006).
[20]J. N. Lee, C. Park, and G. M. Whitesides, "Solvent compatibility of poly(dimethylsiloxane)-based microfluidic devices," Anal. Chem. **75**(23), 6544–6554 (2003).
[21]J. B. Haun and D. A. Hammer, "Quantifying nanoparticle adhesion mediated by specific molecular interactions," Langmuir **24**(16), 8821–8832 (2008).
[22]O. Khan and M. Sefton, "Endothelial cell behaviour within a microfluidic mimic of the flow channels of a modular tissue engineered construct," Biomed. Microdevices **13**(1), 69–87 (2011).
[23]J.-C. Murciano *et al.*, "ICAM-directed vascular immunotargeting of antithrombotic agents to the endothelial luminal surface," presented in part as posters at the American Thoracic Society (ATS) Meeting, May 5–10, 2000, Toronto, ON, Canada (2003), Vol. 101, pp. 3977–3984.
[24]M. Rémy *et al.*, "*In vitro* and in situ intercellular adhesion molecule-1 (ICAM-1) expression by endothelial cells lining a polyester fabric," Biomaterials **20**(3), 241–251 (1999).
[25]S. Muro *et al.*, "Endothelial targeting of high-affinity multivalent polymer nanocarriers directed to intercellular adhesion molecule 1," J. Pharmacol. Exp. Ther. **317**(3), 1161–1169 (2006).
[26]C. Shipman, "Evaluation of 4-(2-hydroxyethyl)-1-piperazineëthanesulfonic acid (HEPES) as a tissue culture buffer," Exp. Biol. Med. **130**(1), 305–310 (1969).
[27]S. Chien, "Molecular basis of rheological modulation of endothelial functions: Importance of stress direction," Biorheology **43**(2), 95–116 (2006).
[28]Y.-S. J. Li, J. H. Haga, and S. Chien, "Molecular basis of the effects of shear stress on vascular endothelial cells," J. Biomech. **38**(10), 1949–1971 (2005).
[29]S. Chien, "Effects of disturbed flow on endothelial cells," Ann. Biomed. Eng. **36**(4), 554–562 (2008).
[30]S. M. Wasserman and J. N. Topper, "Adaptation of the endothelium to fluid flow: *In vitro* analyses of gene expression and *in vivo* implications," Vasc. Med. **9**(1), 35–45 (2004).
[31]A. M. Malek and S. Izumo, "Mechanism of endothelial cell shape change and cytoskeletal remodeling in response to fluid shear stress," J. Cell Sci. **109**(4), 713–726 (1996).
[32]A. Wong, T. Pollard, and I. Herman, "Actin filament stress fibers in vascular endothelial cells *in vivo*," Science **219**(4586), 867–869 (1983).
[33]D. W. Kim, A. I. Gotlieb, and B. L. Langille, "*In vivo* modulation of endothelial F-actin microfilaments by experimental alterations in shear stress," Arterioscler., Thromb., Vasc. Biol. **9**(4), 439–445 (1989).
[34]C. G. Galbraith, R. Skalak, and S. Chien, "Shear stress induces spatial reorganization of the endothelial cell cytoskeleton," Cell Motil. Cytoskeleton **40**(4), 317–330 (1998).
[35]N. Prasain and T. Stevens, "The actin cytoskeleton in endothelial cell phenotypes," Microvasc. Res. **77**(1), 53–63 (2009).
[36]K. Burridge and E. S. Wittchen, "The tension mounts: Stress fibers as force-generating mechanotransducers," J. Cell Biol. **200**(1), 9–19 (2013).
[37]P. F. Davies, "Flow-mediated endothelial mechanotransduction," Physiol. Rev. **75**(3), 519–560 (1995).
[38]S. Tojkander, G. Gateva, and P. Lappalainen, "Actin stress fibers—Assembly, dynamics and biological roles," J. Cell Sci. **125**(8), 1855–1864 (2012).
[39]K. Katoh, Y. Kano, and S. Ookawara, "Role of stress fibers and focal adhesions as a mediator for mechano-signal transduction in endothelial cells in situ," Vasc. Health Risk Manag. **4**(6), 1273–1282 (2008).
[40]P. S. Acharya *et al.*, "Fibroblast migration is mediated by CD44-dependent TGFβ activation," J. Cell Sci. **121**(9), 1393–1402 (2008).
[41]S. R. Thomas, P. K. Witting, and G. R. Drummond, "Redox control of endothelial function and dysfunction: Molecular mechanisms and therapeutic opportunities," Antioxid. Redox Signaling **10**(10), 1713–1766 (2008).
[42]See supplementary material at http://dx.doi.org/10.1063/1.4936672 for studies showing the change in surface ICAM-1 expression for BAOECs when treated with TNF-α from the basal and apical side of the cell separately, and results on targeted binding of anti-ICAM-1 coated particles of 1 μm size.
[43]J. D. van Buul *et al.*, "Inside-out regulation of ICAM-1 dynamics in TNF-α-activated endothelium," PLoS one **5**(6), e11336 (2010).
[44]H. Klingberg *et al.*, "The influence of flow, shear stress and adhesion molecule targeting on gold nanoparticle uptake in human endothelial cells," Nanoscale **7**(26), 11409–11419 (2015).
[45]J.-J. Chiu *et al.*, "Shear stress increases ICAM-1 and decreases VCAM-1 and E-selectin expressions induced by tumor necrosis factor-α in endothelial cells," Arterioscler., Thromb., Vasc. Biol. **24**(1), 73–79 (2004).

[46]S. Srigunapalan *et al.*, "A microfluidic membrane device to mimic critical components of the vascular microenvironment," Biomicrofluidics **5**(1), 013409 (2011).
[47]A. Burke-Gaffney and P. G. Hellewell, "Tumour necrosis factor-alpha-induced ICAM-1 expression in human vascular endothelial and lung epithelial cells: Modulation by tyrosine kinase inhibitors," Br. J. Pharmacol. **119**(6), 1149–1158 (1996).
[48]A. Thomas, J. Tan, and Y. Liu, "Characterization of nanoparticle delivery in microcirculation using a microfluidic device," Microvasc. Res. **94**(0), 17–27 (2014).
[49]A. J. Calderon *et al.*, "Flow dynamics, binding and detachment of spherical carriers targeted to ICAM-1 on endothelial cells," Biorheology **46**(4), 323–341 (2009).
[50]J. Tan, A. Thomas, and Y. Liu, "Influence of red blood cells on nanoparticle targeted delivery in microcirculation," Soft Matter **8**(6), 1934–1946 (2012).
[51]P. Charoenphol, R. B. Huang, and O. Eniola-Adefeso, "Potential role of size and hemodynamics in the efficacy of vascular-targeted spherical drug carriers," Biomaterials **31**(6), 1392–1402 (2010).
[52]S. E. Goldblum, X. Ding, and J. Campbell-Washington, "TNF-alpha induces endothelial cell F-actin depolymerization, new actin synthesis, and barrier dysfunction," Am. J. Physiol. **264**(4 Pt 1), 894–905 (1993).
[53]J. Peng *et al.*, "Protein kinase C-alpha signals P115RhoGEF phosphorylation and RhoA activation in TNF-alpha-induced mouse brain microvascular endothelial cell barrier dysfunction," J. Neuroinflammation **8**(1), 28 (2011).
[54]J. A. G. McKenzie and A. J. Ridley, "Roles of Rho/ROCK and MLCK in TNF-α-induced changes in endothelial morphology and permeability," J. Cell. Physiol. **213**(1), 221–228 (2007).
[55]S. Y. Yuan, "Protein kinase signaling in the modulation of microvascular permeability," Vasc. Pharmacol. **39**(4–5), 213–223 (2002).
[56]D. Schulte *et al.*, "Stabilizing the VE-cadherin–catenin complex blocks leukocyte extravasation and vascular permeability," The EMBO Journal **30**, 4157–4170 (2011).
[57]F. T. Arce *et al.*, "Regulation of the micromechanical properties of pulmonary endothelium by S1P and thrombin: Role of cortactin," Biophys. J. **95**(2), 886–894 (2008).
[58]S. Y. Yuan and R. R. Rigor, "Signaling mechanisms in the regulation of endothelial permeability," *Regulation of Endothelial Barrier Function* (Morgan & Claypool Life Sciences, San Rafael, CA, 2010), Chap. 5.
[59]B. Wójciak-Stothard *et al.*, "Regulation of TNF-α-induced reorganization of the actin cytoskeleton and cell-cell junctions by Rho, Rac, and Cdc42 in human endothelial cells," J. Cell. Physiol. **176**(1), 150–165 (1998).
[60]M. C. Coll Ferrer *et al.*, "ICAM-1 targeted nanogels loaded with dexamethasone alleviate pulmonary inflammation," PLoS One **9**(7), e102329 (2014).
[61]T. Bhowmick *et al.*, "Effect of flow on endothelial endocytosis of nanocarriers targeted to ICAM-1," J. Controlled Release **157**(3), 485–492 (2012).
[62]A. J. Calderon *et al.*, "Optimizing endothelial targeting by modulating the antibody density and particle concentration of anti-ICAM coated carriers," J. Controlled Release **150**(1), 37–44 (2011).